A NEW EXOTIC STATE IN AN OLD MATERIAL: A TALE OF SmB_6

M. Dzero [a], *V. Galitski* [b*]

[a] *Department of Physics, Kent State University, Kent, OH 44242, USA*

[b] *Condensed Matter Theory Center and Department of Physics,
University of Maryland, College Park, MD 20742, USA*

Dedicated to the memory of Professor Anatoly Larkin

We review current theoretical and experimental efforts to identify a novel class of intermetallic $4f$ and $5f$ orbital materials in which strong interactions between itinerant and predominately localized degrees of freedom gives rise to a bulk insulating state at low temperatures, while the surface remains metallic. This effect arises due to inversion of even-parity conduction bands and odd-parity very narrow f-electron bands. The number of band inversions is mainly determined by the crystal symmetry of a material and the corresponding degeneracy of the hybridized f-electron bands. For an odd number of band inversions, the metallic surface states are chiral and therefore remain robust against disorder and time-reversal invariant perturbations. We discuss a number of unresolved theoretical issues specific to topological Kondo insulators and outline experimental challenges in probing the chiral surface states in these materials.

1. INTRODUCTION

In the past ten years, researchers have been fascinated with a peculiar kind of materials: topological insulators [1–6]. These materials host spin-momentum-locked (i. e., chiral) metallic surface states, which allow them to remain robust to time-reversal invariant perturbations [7–13]. In addition, these materials, when brought into contact with s-wave superconductors, support Majorana fermions that are their own antiparticles [14, 15]. The combination of these properties makes topological insulators promising platforms for spintronics and quantum computing applications. At the same time, these materials, which have been proved to possess topologically protected metallic surface states, have significant bulk conductivity [16–19]. In this sense they are therefore not ideal topological insulators.

One promising route to the discovery of ideal topological insulators is to examine materials with strong electron–electron interactions. First, the electron correlations may fully suppress the bulk conductivity. Second, electronic interactions may significantly enhance

the spin–orbit coupling, which is responsible for the inversion of the bands with opposite parity. In weakly correlated Bi-based topological insulators, spin–orbit coupling inverts the s- and p-bands. In correlated topological insulators, we expect bands with higher orbital numbers, either p- and d-orbitals or s-, d-, and f-orbitals, to invert. For example, a topological Mott insulating state has been theoretically predicted for d-orbital pyrochlore irridates within the extended Hubbard model on a honeycomb lattice [20–24], while inversion between Os d-bands and Ce f-bands leads to a topological insulator in filled skutterudites [25] and the general two-dimensional Kondo system where topological insulating state is hidden inside the ferromagnetic metallic state [26]. It is also worth mentioning the theoretical realization of various interaction-driven topological phases in ultracold atom systems and graphene [27–29].

In this article, we focus on recent theoretical and experimental breakthroughs in the search for the ideal topological insulator in higher orbital systems. The special attention is given to the already existing f-orbital materials [30], such as CeNiSn, $Ce_3Bi_4Pt_3$, YbB_{12}, and SmB_6. These materials, which are called Kondo insulators, have all the necessary features needed for realizing topological behavior: strong spin–orbit coupling, strong electron–electron interactions, and orbitals with

*E-mail: galitski@physics.umd.edu

Table. Strength of the Hubbard interaction U and spin–orbit coupling λ depending on the orbital state type

	$4d$	$5d$	$4f$	$5f$
U, eV	1.5	1	1.7	2.1
λ, eV	$0.1,\ldots,0.2$	$0.4,\ldots,0.6$	$0.7,\ldots,1$	$1,\ldots,2$

opposite parity (see Table). The strong spin–orbit coupling is inherent in f-electron systems and guarantees the inversion of the bands at the high-symmetry points in the Brillouin zone. The predominantly localized character of the f-electrons furnishes a strong Coulomb repulsion between them, while hybridization between the even-parity conduction electrons and f-electrons leads to the emergence of the hybridization gap. Interestingly enough, the onset of the hybridization gap, observed by Raman spectroscopy in some Kondo insulators, has clear features of a second-order phase transition. In any case, the opening of the hybridization gap does not guarantee an insulating gap, of course. But in Kondo insulators, the total number of conduction and f-electrons per unit cell is even and, consequently, it immediately follows that Kondo insulators are strongly correlated analogues of band insulators.

This article is organized as follows. In the next section, we review the theoretical models that lead to the original prediction [31] that Kondo insulators with tetragonal or orthorhombic crystalline symmetries can naturally become a host to topologically protected metallic surface states. Section 3 is devoted to the review of recent experimental and theoretical efforts toward the understanding of the physics of cubic topological Kondo insulators and, specifically, SmB_6. In Sec. 4, we discuss open questions, the answers to which will deepen our understanding of topological Kondo insulators. We summarize the current status of the field and present our conclusions in Sec. 5.

2. THEORIES OF TOPOLOGICAL KONDO INSULATORS

In this section, we review the recent theories of topological Kondo insulators. We consider the case where the f-ion is in tetragonal crystalline field environment and review the theoretical results obtained for this case first. We then proceed with the discussion of the theories for cubic topological Kondo insulators, which are relevant for SmB_6, YbB_{12}, and $Ce_3Bi_4Pt_3$ materials.

2.1. Tetragonal topological Kondo insulators

The minimal model of Kondo insulators must involve conduction and strongly correlated f-electrons as well as hybridization between them. Before we write the corresponding periodic Anderson model, we need to specify the f-electron states. Since most of the tetragonal systems that are insulating or semi-metallic contain Ce, we consider the model for the Ce ion in a state with the total angular momentum $J = 5/2$. The six-fold degenerate multiplet is then split into the three Kramers doublets with the eigenvectors written conveniently in terms of the eigenvectors of the angular momentum projection operator $\hat{J}_z$ as [32]

$$
\begin{aligned}
|\mu = \pm 1\rangle &= |\pm 1/2\rangle, \\
|\mu = \pm 2\rangle &= \cos\alpha|\pm 5/2\rangle - \sin\alpha|\mp 3/2\rangle, \quad (1) \\
|\mu = \pm 3\rangle &= \sin\alpha|\pm 5/2\rangle + \cos\alpha|\mp 3/2\rangle,
\end{aligned}
$$

where the angle α determines the degree of mixing between the corresponding orbitals. These eigenvectors can be conveniently expressed in terms of the spin part of the electron wave function χ_σ as

$$
|\mu\rangle = \sum_{M=-5/2}^{5/2} B_{\mu M}\sqrt{4\pi} \sum_{m=-3}^{3} A_{lm\sigma}^{M}|m,l\rangle\chi_\sigma, \quad (2)
$$

where $A_{lm\sigma}^{M}$ are the Clebsch–Gordan coefficients and $B_{\mu M}$ are some known constants determined from the crystalline electric field (CEF) potential.

The minimal model Hamiltonian for the tetragonal Kondo insulator then takes the form [31–33]

$$
\begin{aligned}
\hat{H} = \sum_{\mathbf{k}\sigma} \xi_{\mathbf{k}}\hat{c}_{\mathbf{k}\sigma}^{\dagger}\hat{c}_{\mathbf{k}\sigma} + \\
+ \sum_{\mathbf{k}\mu} \varepsilon_{\mathbf{k}}^{(f)} \hat{f}_{\mathbf{k}\mu}^{\dagger}\hat{f}_{\mathbf{k}\mu} + \sum_{\mathbf{k}\mu\sigma} \left(V_{\mathbf{k}\sigma\mu}^{*}\hat{f}_{\mathbf{k}\mu}^{\dagger}\hat{c}_{\mathbf{k}\sigma} + \text{H.c.} \right) + \\
+ \frac{1}{2}U_{ff} \sum_{i;\mu\neq\mu'} \hat{f}_{i\mu}^{\dagger}\hat{f}_{i\mu}\hat{f}_{i\mu'}^{\dagger}\hat{f}_{i\mu'}, \quad (3)
\end{aligned}
$$

where $\hat{c}_{\mathbf{k}\sigma}^{\dagger}$ creates an electron in the conduction band in a plane-wave state with the momentum $\mathbf{k}$, spin $\sigma = \uparrow, \downarrow$ and energy $\xi_{\mathbf{k}}$ (relative to the chemical potential of the conduction band), while $\hat{f}_{\mathbf{k}\mu}^{\dagger}$ creates an f-electron in a state with momentum $\mathbf{k}$ and the multiplet component μ in (1) and the energy $\varepsilon_{\mathbf{k}}^{(f)}$. We note that the bandwidth of the f-electrons is much smaller than the one for the conduction electrons. The third term in (3) describes the momentum-dependent hybridization between the conduction and f-electrons, while the last terms accounts for strong local correlations between the f-electrons on site i. This last terms is important because it leads to the local moment formation.

It is very intuitive that the momentum dependence of the hybridization amplitude determines the anisotropy of the hybridization gap, which becomes an insulating gap if the total number of electrons per unit cell is even. Formally, the momentum dependence of $V_{\mathbf{k}\mu\sigma}$ can be written in terms of the spherical harmonic functions [32, 34]:

$$V_{\mathbf{k}\mu\sigma} = \sum_{M=-5/2}^{5/2} B_{\mu M}\sqrt{4\pi}V_{kl}\sum_{m=-3}^{3} A_{lm\sigma}^{M}\tilde{Y}_{l}^{m}(\mathbf{k}), \quad (4)$$

where V_{kl} are the matrix elements, which can be expressed in terms of the corresponding Slater–Koster matrix elements [35]. We note that the values of the momentum in (4) are defined everywhere in the Brillouin zone and

$$\tilde{Y}_{l}^{m}(\mathbf{k}) = \frac{1}{Z}\sum_{\mathbf{R}\neq\mathbf{0}} Y_{l}^{m}(\hat{\mathbf{R}})e^{i\mathbf{k}\cdot\mathbf{R}} \quad (5)$$

is a tight-binding generalization of the spherical Harmonics that preserves the translational symmetry of the hybridization, $V_{\mathbf{k}} = V_{\mathbf{k}+\mathbf{G}}$, where $\mathbf{G}$ is a reciprocal lattice vector [31, 34]. Here, $\mathbf{R}$ are the positions of the Z nearest-neighbor sites around the magnetic ion.

The low-energy properties of the model in (3) can be analyzed by the using the following conjecture: the effect of the local correlations between the f-electrons leads to the renormalization of the hybridization amplitude and a shift of the f-energy level:

$$\varepsilon_{\mathbf{k}\mu}^{(f)} \to \tilde{\varepsilon}_{\mathbf{k}\mu}^{(f)} = Z_{\mathbf{k}\mu}\left(\varepsilon_{\mathbf{k}\mu}^{(f)} + \Sigma_{\mu\mu}(\mathbf{k},\omega=0)\right),$$

$$|V_{\mathbf{k}\mu\sigma}| \to |\tilde{V}_{\mathbf{k}\mu\sigma}| = \sqrt{Z_{\mathbf{k}\mu}}|V_{\mathbf{k}\mu\sigma}|, \quad (6)$$

where the renormalization factor $Z_{\mathbf{k}\mu}$ is determined by the f-electron self-energy part $\Sigma_{\mu\mu}(\mathbf{k},\omega)$:

$$Z_{\mathbf{k}\mu} = \left[1 - \frac{\partial\Sigma_{\mu\mu}(\mathbf{k},\omega)}{\partial\omega}\right]_{\omega=0}^{-1}. \quad (7)$$

Then the low-energy model can be diagonalized, yielding a band structure that consists of two doubly degenerate bands separated by the momentum-dependent energy gap $\Delta_{\mathbf{k}}$ given by

$$\Delta_{\mathbf{k}}^{2} = \frac{1}{2}\mathrm{Tr}[V_{\mathbf{k}}^{\dagger}V_{\mathbf{k}}], \quad (8)$$

where we suppressed the spin and orbital indices for brevity. Since the total number of electrons per unit cell is even, the lowest two bands are guaranteed to be fully occupied, and we have a band insulator if $\Delta_{\mathbf{k}}$ does not have nodes anywhere in the Brillouin zone

apart from the high-symmetry points, where it vanishes because $V_{-\mathbf{k};\mu\sigma} = -V_{\mathbf{k},\mu,\sigma}$. Analysis of the momentum dependence of $\Delta_{\mathbf{k}}$ shows that for $\mu = \pm2, \pm3$, the function $\Delta_{\mathbf{k}}$ vanishes at $k_z = \pm k$, i.e., the gap has two point nodes [32]. Therefore, hybridization and insulating gap always open for $\mu = \pm1/2$, corresponding to a ground-state multiplet with $J_z = \pm1/2$. We note in passing that for systems with lower symmetry (i.e., orthorhombic), the ground-state Kramers doublet is given by a linear combination of states (1). In this case, although $J_z = \pm1/2$ is nodeless, it can be shown that the hybridization gap acquires nodes at some finite values of the momentum $\mathbf{k}$ (see the discussion in Ref. [32] for the details).

The parity at a high-symmetry point can be determined by $\delta_m = \mathrm{sign}(\xi_{\mathbf{k}_m^*} - \tilde{\varepsilon}_{\mathbf{k}_m^*}^{(f)})$ [1, 6, 31, 34]. Four independent Z_2 topological indices $(\nu_0; \nu_1\nu_2\nu_3)$ [36], one strong ($a = 0$) and three weak indices ($a = 1, 2, 3$) can be constructed from δ_m as follows.

(i) The strong topological index is the product of all eight δ_ms:

$$I_{STI} = (-1)^{\nu_0} = \prod_{m=1}^{8} \delta_m = \pm1.$$

(ii) By setting $k_j = 0$ (where $j = x, y, z$), three high-symmetry planes $P_j = \{\mathbf{k} : k_j = 0\}$ are formed that contain four high-symmetry points each. The product of the parities at these four points defines the corresponding weak topological index

$$I_{WTI}^{a} = (-1)^{\nu_a} = \prod_{\mathbf{k}_m \in P_j} \delta_m = \pm1, \quad a = 1, 2, 3,$$

with integers corresponding to the axes x, y, and z. The existence of the three weak topological indices in 3D is related to a Z_2 topological index for 2D systems (a weak 3D topological insulator is similar to a stack of 2D Z_2 topological insulators). Because there are three independent ways to stack 2D layers to form a 3D system, the number of independent weak topological indices is also three. A conventional band insulator (BI) has all of the four indices, $I_{STI} = I_{WTI}^{x} = I_{WTI}^{y} = I_{WTI}^{z} = +1$ or equivalently (0;000). An index $I = (-1)$ ($\nu_a = 1$) indicates a Z_2 topological state with an odd number of surface Dirac modes. In a tetragonal Kondo insulator the inversion index δ_m of a particular high-symmetry point m is negative if the conduction band is below the f-band: $\xi_{\mathbf{k}_m^*} < \tilde{\varepsilon}_{\mathbf{k}_m^*}^{(f)}$. Hence, if $\xi_{\mathbf{k}_m=0} < \tilde{\varepsilon}_{\mathbf{k}_m=0}^{(f)}$ at the Γ point, while the remaining high-symmetry points remain inert, $\xi_{\mathbf{k}_m\neq\mathbf{0}} > \tilde{\varepsilon}_{\mathbf{k}_m^*}^{(f)}$, then $I_{STI} = -1$, and therefore the tetragonal Kondo insulator is a strong topological insulator (STI), robust against disorder (Fig. 1 a).
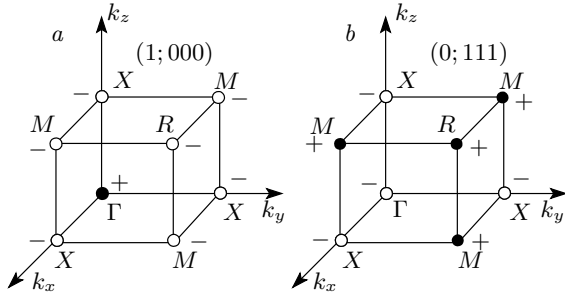
Fig. 1. Two topologically distinct states can be realized in our model of tetragonal topological Kondo insulators. The first one has the topological invariant $\nu = (1; 000)$ and corresponds to a strong topological insulator. The second one has the topological invariant $\nu = (0; 111)$

Fig. 2. Large-N mean-field theory results for the topological Kondo insulator [43]. (a) Phase diagram calculated for a doubly degenerate f-ion multiplet, $N = 2$, as a function of the average electronic occupation of the f-level, $0 \le n_f \le 1$. In the local moment regime, $n_f \approx 1$, the weak topological insulator (WTI) with the topological invariant $\nu = (0; 111)$ is realized. In the mixed-valence regime, $n_f \sim 1$, the Kondo insulator is a strong topological insulator (STI) with the topological invariant given by $\nu = (1; 111)$. When the hybridization between the conduction and f-electrons becomes even stronger, the material is a trivial or band insulator (BI), $\nu = (0; 000)$. (b) and (c) Phase diagram for $N = 4$ and $N = 6$ correspondingly. Note that the WTI state disappears as the degeneracy of the f-multiplet increases

Weak topological insulators (WTIs) and topologically trivial insulators can in principle be found for different band structures and different values of $\tilde{\varepsilon}^{(f)}_{\mathbf{k}^*_m = 0}$ (Fig. 1 b).

We can go beyond the phenomenological description described above and resort to a more microscopic approach. Specifically, we can consider the limit $U_{ff} \to \infty$ and work in the restricted phase space by projecting out the doubly occupied f-states. Formally, this is accomplished by introducing the slave boson operators [37–41]. Then the mean-field analysis of the resulting model can be made by replacing the slave boson operators by a number, which must be determined self-consistently. The mean-field theory is controlled by the degeneracy of the f-orbital multiplet. The large-N mean-field for analysis the tetragonal Kondo insulator has been done in [42] and also in [43]. The results of the slave-boson mean-field theory generally agree with the phenomenological approach for $N = 2$ (Fig. 2 a). In Ref. [43], the mean-field diagram has also been obtained for $N > 2$ (Fig. 2 b,c). Interestingly, it was found that the WTI state is suppressed as the degeneracy of the f-multiplet increases, and only the STI state is present for $N = 6$. This result indicates that the STI state should be preferred for higher-symmetry, i. e., cubic, systems. We return to this observation when we discuss the cubic topological Kondo insulators below.

The phenomenological and mean-field models discussed so far assume that the interaction between f-electrons is infinitely large. How do the results change if we consider finite values of U_{ff}? Can we study the evolution of the topological state as a function of U_{ff}? In other words, can a Kondo insulator be adiabatically connected to a non-interaction band insulator? This and related questions have been recently addressed by Werner and Assaad [44] by using the dynamical mean-field theory (DMFT) to analyze the 2D Kondo insulators.
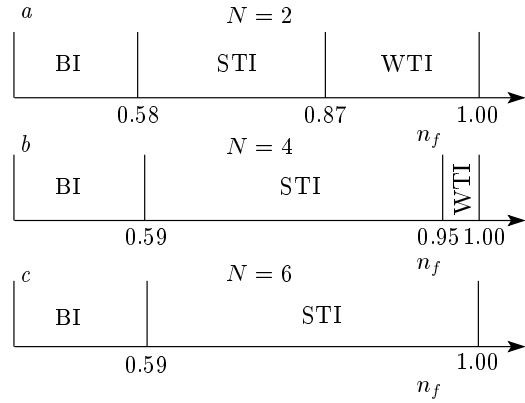
The physical properties of the model described by the Anderson lattice Hamiltonian in (3) can be captured, in particular, by the single-particle propagators. The self-energy corrections in the single-particle correlation functions are governed by the Hubbard repulsion between the f-electrons. Generally, the f-electron self-energy part depends on both momentum and frequency. Within the DMFT, however, a single f-electron site version of the lattice model in (3) is considered, which allows computing the single-particle and higher-order correlation functions exactly [45]. Consequently, the self-energy parts, which encode the correlation between the f-electrons, are all momentum independent. Then the self-energy parts for the conduction and f-electrons corresponding to the lattice problem can be determined self-consistently from the solution of the impurity problem.

Interestingly, Werner and Assaad have found [44] that increasing the strength of the Hubbard interaction leads to a series of transitions from the normal insulator
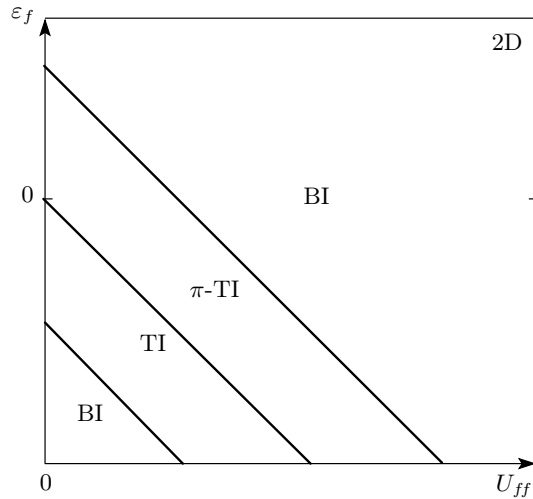
Fig. 3. Dynamical mean field theory phase diagram for the 2D Kondo insulator (adopted from Ref. [44]). As the strength of the Hubbard interaction U_{ff} between the f-electrons increases, there are three topologically distinct insulating states. A band insulator (BI) is realized for small (compared to the conduction electron bandwidth) values of U_{ff}. A topological insulator (TI) with band inversion at the Γ point sets in for intermediate values of U_{ff}. When the interaction strength U_{ff} increases further, this state is superseded by a topologically nontrivial π-TI state: in this state, bands of the opposite parity invert at the X points of the 2D Brillouin zone. At the boundaries between topologically distinct states, the system is semimetallic
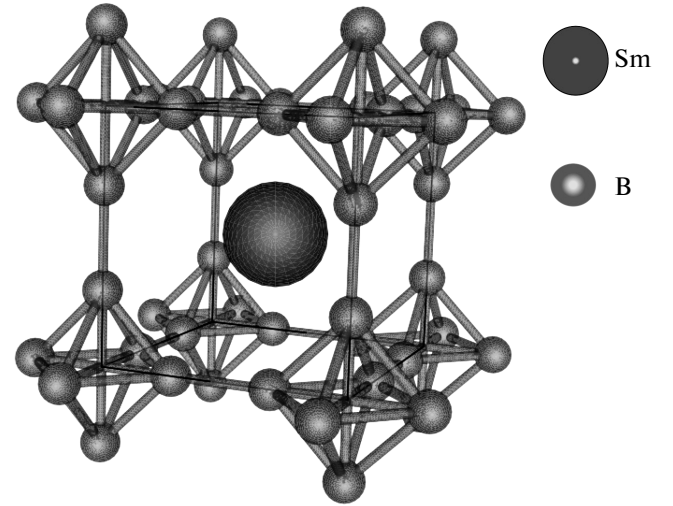

Fig. 4. Crystal structure of SmB_6. The Sm ions are at the center of the unit cell and are surrounded by octahedrons of boron ions located at the corners of the unit cell

(small U_{ff}) into a STI with the in-gap state crossing the Fermi level at the Γ point, and then into another STI, in which the in-gap states cross the Fermi level at the X point (Fig. 3). These results clearly indicate that the previously developed concept of adiabatic connection between uncorrelated band insulators and strongly correlated Kondo insulators [46] does not hold at least for the two-dimensional Kondo lattice. It remains to be verified, of course, whether this conclusion holds for a 3D Kondo insulator. In conclusion, we note that true tetragonal Kondo insulators are still to be experimentally discovered, because until now, the Ce-based tetragonal "Kondo insulators", such as CeNiSn [47] and $CeRuSn_6$ [48], become semimetals upon improving the sample quality.

2.2. Cubic topological Kondo insulators

Kondo insulators consistently show insulating behavior in transport measurements — most notably, SmB_6, YbB_{12}, and $Ce_3Bi_4Pt_3$ — are all cubic. In this section, we review the recent theories of cubic topological Kondo insulators, using samarium hexaboride as a specific example [49–51]. We note, however, that the model that we discuss below should also hold for $Ce_3Bi_4Pt_3$, although some parameters can be different.

The magnetic valence configuration of the Sm ion corresponds to the state with the total angular momentum $J = 5/2$. The six-fold degenerate Sm multiplet is split by cubic crystal fields into the Γ_7 Kramers doublet and a Γ_8 quartet. Consequently, the eigenstates of the cubic crystalline field Hamiltonian are given by

$$
|\Gamma_7, \pm\rangle = \sqrt{\frac{1}{6}} | \pm 5/2 \rangle - \sqrt{\frac{5}{6}} | \mp 3/2 \rangle,
$$

$$
|\Gamma_8^{(1)}, \pm\rangle = \sqrt{\frac{5}{6}} | \pm 5/2 \rangle + \sqrt{\frac{1}{6}} | \mp 3/2 \rangle, \tag{9}
$$

$$
|\Gamma_8^{(2)}, \pm\rangle = | \pm 1/2 \rangle.
$$

If Γ_7 is the ground-state multiplet, the system is a semimetal because the hybridization gap has nodes in the Brillouin zone [32]. Thus, for an insulating state, we necessarily need Γ_8 to be the ground-state multiplet. This appears to be indeed the case for SmB_6 (as well as for $Ce_3Bi_4Pt_3$), as is evidenced by inelastic neutron scattering experiments and Raman spectroscopy [52–55].

SmB_6 has a cubic CsCl-like crystal structure (Fig. 4), with the B_6 clusters located at the center of the unit cell. From band-theory calculations [50, 56], the B_6 clusters act as spacers that mediate electron

hopping between Sm sites, but are otherwise inert. In addition to the band structure results, X-ray photoemission spectroscopy (XPS) of SmB_6 [54] indicates that the conduction bands that hybridize with the localized $4f$-orbitals are $5d$-states, which form electron pockets around the X points. In particular, the physics of the $4f$-orbitals is governed by valence fluctuations involving electrons of the Γ_8 quartet and the conduction e_g-hole states, $4f^5 \rightleftharpoons 4f^6 + h$. The conduction states must be $d_{x^2-y^2}$ and $d_{3z^2-r^2}$ orbitals of the e_g symmetry. Since the lowest-lying state must be a quartet, we immediately conclude that the band inversion occurs an odd number of times and the cubic Kondo insulator must be a strong topological insulator for a moderate value of the hybridization [51]. Indeed, at the Γ point, both d and f-bands remain four-fold degenerate, such that the Γ point remains topologically inert.

Recently, Takimoto [49] performed the low-energy analysis of the Anderson Kondo lattice model in (3) properly generalized to take the realistic band structure of SmB_6 into account. Specifically, the conduction and f-electron spectrum have been derived using the tight-binding approximation to the next-nearest-neighbor approximation. We emphasize that the next-nearest-neighbor hopping is needed in order to obtain the minimum of the conduction bands at the X points of the Brillouin zone. The hybridization part of the Hamiltonian has also been derived using the tight-binding approximation restricted to the nearest neighbors only. This approximation can be justified by noting that the orbital momentum $\Delta l = \pm 1$ is transferred from the conduction d-states to the f-states in the process of hybridization. The phenomenological analysis similar to the one in Ref. [31] of the resulting model shows that SmB_6 is a strong topological insulator. An important conclusion drawn from the results in Ref. [49] is that as a consequence of the band inversion at the X points, there are three Dirac cones on the surfaces perpendicular to the main symmetry axes. A subsequent first-principle study based on the local density approximation (LDA) plus the Gutzwiller method [50] has confirmed the results of the phenomenological theory [49].

Most recently, Alexandrov, Dzero, and Coleman (ADC) formulated a general model for the cubic topological Kondo insulators [51]. The ADC model for the three-dimensional Kondo insulator can be derived from an effective ($U_{ff} \to \infty$) model for the one-dimensional Kondo insulator by applying a series of unitary transformations. Specifically, we consider the quartet of f- and d-holes described by an orbital and a spin in-

dex, denoted by the combination $\lambda \equiv (a, \sigma)$ ($a = 1, 2$, $\sigma = \pm 1$). Consequently, the d- and f-states are then described by the eight-component spinor

$$\Psi_j = \begin{pmatrix} d_\lambda(j) \\ X_{0\lambda}(j) \end{pmatrix}, \qquad (10)$$

where $d_\lambda(j)$ destroys a d-hole at site j, while $X_{0\lambda}(j) = |4f^6\rangle\langle 4f^5, \lambda|$ is the Hubbard operator that destroys an f-hole at site j. The tight-binding Hamiltonian describing the hybridized f–d system is then

$$H = \sum_{i,j} \Psi_\lambda^\dagger(i) h_{\lambda\lambda'}(\mathbf{R}_i - \mathbf{R}_j) \Psi_{\lambda'}(j), \qquad (11)$$

where the nearest hopping matrix has the structure

$$h(\mathbf{R}) = \begin{pmatrix} h^d(\mathbf{R}) & V(\mathbf{R}) \\ V^\dagger(\mathbf{R}) & h^f(\mathbf{R}) \end{pmatrix}. \qquad (12)$$

Here, the diagonal elements describe hopping within the d- and f-quartets and the off-diagonal parts describe the hybridization between them, and $\mathbf{R} \in (\pm\hat{\mathbf{x}}, \pm\hat{\mathbf{y}}, \pm\hat{\mathbf{z}})$ is the vector linking nearest neighbors. The various matrix elements simplify for hopping along the z axis, where they become orbitally and spin diagonal:

$$h^l(\mathbf{z}) = t^l \begin{pmatrix} 1 & \\ & \eta_l \end{pmatrix}, \quad V(\mathbf{z}) = iV \begin{pmatrix} 0 & \\ & \sigma_z \end{pmatrix}. \qquad (13)$$

Here, $l = d, f$ and η_l is the ratio of orbital hopping elements. In the foregoing, the overlap between the $\Gamma_8^{(1)}$ orbitals that extend perpendicular to the z axis is neglected, since the hybridization is dominated by the overlap of the the $\Gamma_8^{(2)}$ orbitals that extend out along the z axis. The hopping matrix elements in the $\mathbf{x}$ and $\mathbf{y}$ directions are then obtained by rotations in the orbital/spin space. Such that

$$h(\mathbf{x}) = U_y h(\mathbf{z}) U_y^\dagger, \quad h(\mathbf{y}) = U_{-x} h(\mathbf{z}) U_{-x}^\dagger,$$

where U_y and U_{-x} respectively denote 90° rotations about the y and negative x axes. By construction, the hopping terms $h^{d,f}(\mathbf{k})$ in Hamiltonian (11) could have been alternatively obtained from the tight-binding approximation within the nearest-neighbor approximation. But it is important to keep in mind that the correct band structure for SmB_6 is still recovered by properly choosing the ratio between the corresponding hopping amplitudes [51].

Furthermore, the Fourier-transformed hopping matrices

$$h(\mathbf{k}) = \sum_{\mathbf{R}} h(\mathbf{R}) e^{-i\mathbf{k}\cdot\mathbf{R}}$$

can be written in the compact form

$$h^l(\mathbf{k}) =$$

$$= t^l \begin{pmatrix} \phi_1(\mathbf{k}) + \eta_l \phi_2(\mathbf{k}) & (1-\eta_l)\phi_3(\mathbf{k}) \\ (1-\eta_l)\phi_3(\mathbf{k}) & \phi_2(\mathbf{k}) + \eta_l \phi_1(\mathbf{k}) \end{pmatrix} + \epsilon^l, \quad (14)$$

where $l = d, f$. Here, ϵ^l are the bare energies of the isolated d- and f-quartets, and

$$\phi_1(\mathbf{k}) = c_x + c_y + 4c_z, \quad \phi_2(\mathbf{k}) = 3(c_x + c_y),$$

$$\phi_3(\mathbf{k}) = \sqrt{3}(c_x - c_y) \quad (c_\alpha = \cos k_\alpha, \alpha = x, y, z).$$

The hybridization is given by

$$V(\mathbf{k}) = \frac{V}{6} \begin{pmatrix} 3(\bar{\sigma}_x + i\bar{\sigma}_y) & \sqrt{3}(\bar{\sigma}_x - i\bar{\sigma}_y) \\ \sqrt{3}(\bar{\sigma}_x - i\bar{\sigma}_y) & \bar{\sigma}_x + i\bar{\sigma}_y + 4\bar{\sigma}_z \end{pmatrix}, \quad (15)$$

where we set $\bar{\sigma}_\alpha = \sigma_\alpha \sin k_\alpha$. Naturally, the hybridization between the even-parity d-states and odd-parity f-states is an odd-parity function of the momentum, $V(\mathbf{k}) = -V(-\mathbf{k})$.

The model in (11) has been analyzed using the slave-boson mean-field approximation and it was shown that the cubic Kondo insulator is an STI, in complete agreement with previous works [49, 50]. Furthermore, ADC have shown that the STI state extends well into the local moment regime, similarly to the results form the large-N theory for tetragonal Kondo insulators (see Fig. 2c). Lastly, we emphasize that the procedure for obtaining the effective model for a cubic Kondo insulator [51] can be easily generalized to various types of conduction orbitals and can therefore be used to analyze the topological properties of the band structure for other cubic Kondo insulators such as YbB_{12} and $Ce_3Bi_4Pt_3$.

3. EXPERIMENT: SAMARIUM HEXABORIDE

In this section, we present a brief overview of experiments on the canonical Kondo insulator SmB_6 [57]. There exists a vast amount of experimental literature on this material, which merits a separate review paper. Here, we focus on discussing the experimental properties of importance for possible realization of topologically protected chiral surface states.

SmB_6 is the first known and most experimentally studied heavy-fermion semiconductor [57]. At high temperatures, SmB_6 is a metal with the magnetic susceptibility showing the Curie–Weiss-like behavior, $\chi \sim 1/T$, signaling the existence of local magnetic moments originating from the Sm f-electrons. At low temperatures $T \ll T_{coh} \approx 50$ K, SmB_6 is a narrow-gap semiconductor with a weakly temperature-dependent magnetic susceptibility [30, 33]. Furthermore, the average electronic occupation of the Sm f states is noninteger and varies between the Sm^{2+} ($4f^6$) and Sm^{3+} ($4f^5 5d$) configurations. This mixed-valence state appears as a result of strong hybridization between the $5d$ and $4f$ Sm electrons [56], which also leads to formation of the hybridization gap $E_h \approx 10$ meV and the many-body insulating gap at $E_g \approx 5$ meV.

Most importantly, the saturation of resistivity at temperatures below $T^* \approx 5$ K was consistently observed independently by many groups [46]. Resistivity saturation was initially interpreted as an extrinsic effect due to formation of the impurity band. However, almost ten years after the initial discovery [57], Allen, Batlogg and Wachter [58] argued based on the Hall coefficient data that the observed values of conductivity were too small for a metallic-like system. Moreover, with subsequent accumulation of the experimental data, it became clear that this is an intrinsic electronic effect, although the controversy regarding the intrinsic or extrinsic origin of the effect remained. This controversy was mainly resolved with pressure experiments [59, 60], which have shown that for the pressure above $p^* \approx 45$ kbar, the SmB_6 recovers its metallic properties. Interestingly, it was observed in [59] that the states contributing to low-T conductivity dominate the transport up to sufficiently high temperatures when the transport gap becomes fully suppressed, which means that these states must be an intrinsic property of the system. Transport measurements under pressure and the applied magnetic field as large as 18 T have shown the negative magnetoresistance $[\Delta\rho(H)/\rho(H = 0)]_{p<p^*} \propto -H^2$ at small pressure, while for pressures above p^*, the magnetoresistance becomes positive and increases as $[\Delta\rho(H)/\rho(H = 0)]_{p>p^*} \propto H^{3/2}$. The activation gap, on the other hand, is very weakly dependent on the magnetic field, which indicates, albeit indirectly, that the Γ_8 quartet is the ground-state multiplet for Sm^{3+} ions, since it has the smallest value of the g-factor, $g_{\Gamma_8} = 2/7$ [61].

Since the seminal paper [58], the puzzle of temperature-independent resistivity below T^* became clearly recognized and its origin remained mysterious for almost thirty years. It was nevertheless widely believed that the low-temperature conductivity in SmB_6 originates primarily from the bulk [62–66] and the surface provides a significantly smaller, if any, contribution to conductivity. From our current perspective, this is quite remarkable, because the first topological insulator could have been discovered almost 30 years ago, well

before the discovery of the integer quantum Hall effect! Nevertheless, it took many years until very recently to ask the question whether the saturation of resistivity below 5 K in SmB_6 is a purely surface effect. Motivated by theoretical work [31], several groups [67–69] have independently addressed the issue of bulk vs surface conductivity. The transport [67], Hall effect [68], and tunneling [69] measurements and the angular-resolved photoemission spectroscopy (ARPES) [70] unambiguously showed that only the surface of SmB_6 is conducting below T^*. Furthermore, the surface metallic states remain surprisingly robust against variations in the surface quality.

Thus, the results of the most recent experiments are manifestly in support of the initial prediction [31] that Kondo insulators host topologically protected surface states. Indeed, the robustness of the surface states and the fact that their appearance is correlated with the emergence of the hybridization gap indicate that SmB_6 is a strong topological insulator [49–51]. However, a combination of high-resolution ARPES and tunneling data are needed to directly confirm the chirality of the metallic surface states in SmB_6.

4. OPEN QUESTIONS

The theoretical and experimental results reviewed by us so far bring up a number of issues that need to be understood. For example, the Raman spectroscopy data [54, 55] seem to indicate that opening of the hybridization gap in SmB_6 happens in a way very similar to a second-order phase transition, i. e., the hybridization gap plays a role of the mean-field order parameter. Typically, mean-field-like transitions assume a well-defined separation of energy scales, just like in conventional superconductors, for example, when the small ratio of the Debye frequency to the Fermi energy renders the mean-field BCS theory extremely reliable. In addition, the mean-field-like onset of hybridization implies that the fluctuations in Kondo insulators are much weaker compared with the metallic heavy-fermion systems, which calls for a better understanding of the fluctuations in heavy-fermion systems.

Theoretically, there is still an open problem of the strong-coupling description of the topological Kondo insulators, similar to the Nozières Fermi-liquid picture of the Kondo ground state [71]. The progress towards the solution of that problem will significantly deepen our understanding of the microscopic structure of the chiral states on the surface of topological Kondo insulators.

Finally, another set of questions concerns Ce-based heavy-fermion semiconductors that order antiferromagnetically. These materials have a tetragonal crystal structure, and it remains to be seen whether antiferromagnetic interactions promote the strong topological insulating state. The same applies to the possibility of the occurence of topological states in heavy-fermion superconductors.

5. CONCLUSIONS AND AN OUTLOOK

As the search for an ideal topological insulator continues, we have come to realizion that at least one ideal topological insulator — samarium hexaboride — has been discovered almost 30 years ago. Current theories of topological Kondo insulators all show that the existence of the chiral surface states in f-orbital semiconductors is one of its fundamental signatures. Moreover, these states exist for the broad range of the system parameters, such as the position of the f-electron chemical potential and the strength of the Hubbard interaction between the f-electrons. For cubic topological Kondo insulators, the only requirement is that the hybridization between the conduction and the f-electrons is strongest at the X or M high-symmetry points in the Brillouin zone. This guarantees an odd number of the band inversions and hence a strong topological insulator.

In recent years, we have witnessed a resurgence of theoretical and experimental activity in the field of heavy-fermion semiconductors, and there remains little doubt that SmB_6 is only the first topological Kondo insulator. The new potential candidates are YbB_{12} and $Ce_3Bi_4Pt_3$ — materials with the physical propeties very similar to those of SmB_6. Topological Kondo insulators would present an ideal platform for in-depth transport studies of chiral surface states. In addition, an interplay between the strong spin–orbit coupling and electron–electron correlations may open a way to study the broader range of effects related to the nontrivial topological structure of the electronic states in these materials. One possible direction is the search for topologically nontrivial states in Kondo semimetals. But the most important challenge lies in developing new ways to probe the chirality of the surface metallic states, whether by spin-polarized tunneling spectroscopy, by Kerr effect measurements, or by radio-frequency and microwave spectroscopy.

Note added in proofs. When we have submitted this paper, several important experimental works on SmB_6 became available. Neupane el al. [72] and Jiang et al. [73] report high-resolution photoemission data. The results of these experiments are in agreement with the theoretical calculations for the surface states [49–51]. What is more, Kim, Xia and Fisk have demonstrated [75] that doping of 3 % of magnetic impurities on the surface of SmB_6 leads to a dramatic increase in resistivity — quite contrary to what is observed for the same amount of doping with non-magnetic ions. This result clearly indicates that surface states remain robust agains the time-reversal invariant perturbations. Most recently, Xia group from UC Irvine have shown [76] the weak antilocalization features in transport properties of the surface states in SmB_6 implying the presence of the strong spin-orbit coupling and, therefore, indirect probe of the surface electrons helicity. Combination of current theoretical and experimental results unambiguously demonstrate that samarium hexaboride is indeed the first ideal topological insulator.

REFERENCES

1. A. B. Bernevig and T. Hughes, *Topological Insulators and Topological Superconductors*, Princeton Univ. Press (2013).

2. M. Z. Hasan and C. L. Kane, Rev. Mod. Phys. **82**, 3045 (2010).

3. X.-L. Qi and S.-C. Zhang, Rev. Mod. Phys. **83**, 1057 (2011).

4. L. Fu, C. L. Kane, and E. J. Mele, Phys. Rev. Lett. **98**, 106803 (2007).

5. J. E. Moore and L. Balents, Phys. Rev. B **75**, 121306(R) (2007).

6. L. Fu and C. L. Kane, Phys. Rev. B **76**, 045302 (2007).

7. R. Roy, Phys. Rev. B **79**, 195322 (2009).

8. D. Hsieh, D. Qian, L. Wray, Y. Xia, Y. S. Hor, R. J. Cava, and M. Z. Hasan, Nature **452**, 970 (2008).

9. Y. Xia, D. Qian, D. Hsieh, L. Wray, A. Pal, H. Lin, A. Bansil, D. Grauer, Y. S. Hor, R. J. Cava, and M. Z. Hasan, Nature Phys. **5**, 398 (2009).

10. P. Roushan, J. Seo, C. V. Parker, Y. S. Hor, D. Hsieh, D. Qian, A. Richardella, M. Z. Hasan, R. J. Cava, and A. Yazdani, Nature **460**, 1106 (2009).

11. T. Zhang, P. Cheng, X. Chen, J. F. Jia, X. C. Ma, K. He, L. L. Wang, H. J. Zhang, X. Dai, Z. Fang, X. C. Xie, and Q. K. Xue, Phys. Rev. Lett. **103**, 266803 (2009).

12. J. Seo, P. Roushan, H. Beidenkopf, Y. S. Hor, R. J. Cava, and A. Yazdani, Nature **466**, 343 (2010).

13. Z. Alpichshev, J. G. Analytis, J. H. Chu, I. R. Fisher, Y. L. Chen, Z. X. Shen, A. Fang, and A. Kapitulnik, Phys. Rev. Lett. **104**, 016401 (2010).

14. C. W. Beenaker, arXiv:1112.1950.

15. T. Stanescu and S. Tewari, arXiv:1302.5433.

16. D.-X. Qu, Y. S. Hor, J. Xiong, R. J. Cava, and N. P. Ong, Science **329**, 821 (2010).

17. N. P. Butch, K. Kirshenbaum, P. Syers, A. B. Sushkov, G. S. Jenkins, H. D. Drew, and J. Paglione, Phys. Rev. B **81**, 241301 (2010).

18. J. G. Analytis, R. D. McDonald, S. C. Riggs, J.-H. Chu, G. S. Boebinger, and I. R. Fisher, Nature Phys. **6**, 960 (2010).

19. J. G. Checkelsky, Y. S. Hor, M.-H. Liu, D.-X. Qu, R. J. Cava, and N. P. Ong, Phys. Rev. Lett. **103**, 246601 (2009).

20. S. Raghu, X.-L. Qi, C. Honerkamp, and S.-C. Zhang, Phys. Rev. Lett. **100**, 156401 (2008).

21. H. M. Guo and M. Franz, Phys. Rev. Lett. **103**, 206805 (2009).

22. D. A. Pesin and L. Balents, Nature Phys. **6**, 376 (2010).

23. X. A. Wan, A. Turner, A. Vishwanath, and S. Y. Savrasov, Phys. Rev. B **83**, 205101 (2011).

24. B.-J. Yang and Y. B. Kim, Phys. Rev. B **82**, 085111 (2010).

25. B. Yan, L. Müchler, X. L. Qi, S. C. Zhang, and C. Felser, Phys. Rev. B **85**, 165125 (2012).

26. T. Yoshida, R. Peters, S. Fujimoto, and N. Kawakami, arXiv:1301.5688.

27. K. Sun, H. Yao, E. Fradkin, and S. A. Kivelson, Phys. Rev. Lett. **103**, 046811 (2009).

28. R. Nandkishore and L. Levitov, Phys. Rev. B **82**, 115124 (2010).

29. K. Sun, W. V. Liu, A. Hemmerich, and S. Das Sarma, Nature Phys. **8**, 67 (2012).

30. G. Aeppli and Z. Fisk, Comm. Condens. Matter Phys. **16**, 155 (1992).

31. M. Dzero, K. Sun, V. Galitski, and P. Coleman, Phys. Rev. Lett. **104**, 106408 (2010).

32. M. Miyazawa and K. Yamada, J. Phys. Soc. Jpn. **72**, 2033 (2003).

33. P. Riseborough, Adv. Phys. **49**, 257 (2000).

34. M. Dzero, K. Sun, P. Coleman, and V. Galitski, Phys. Rev. B **85**, 045130 (2012).

35. K. Takegahara, Y. Aoki, and A. Yanase, J. Phys. C **13**, 583 (1980).

36. A. Kitaev, arXiv:0901.2686v2.

37. S. E. Barnes, J. Phys. F **6**, 1375 (1976).

38. N. Read and D. M. Newns, J. Phys. C **16**, 3237 (1983).

39. P. Coleman, Phys. Rev. B **29**, 3035 (1984).

40. Z. Tesanović and O. Valls, Phys. Rev. B **34**, 1918 (1987).

41. D. M. Newns and N. Read, Adv. Phys. **36**, 799 (1987).

42. M. T. Tran, T. Takimoto, and K. S. Kim, Phys. Rev. B **85**, 125128 (2012).

43. M. Dzero, Eur. Phys. J. B **85**, 297 (2012).

44. J. Werner and F. F. Assaad, arXiv:1302.1874.

45. A. Georges, G. Kotliar, W. Krauth, and M. J. Rozenberg, Rev. Mod. Phys. **68**, 13 (1996).

46. C. M. Varma, in *Valence Instabilities and Related Narrow Band Phenomena*, ed. by R. D. Parks, Plenum Press, New York (1977).

47. K. Izawa, T. Suzuki, T. Fujita, T. Takabatake, G. Nakamoto, H. Fujii, and K. Maezawa, Phys. Rev. B **59**, 2599 (1999).

48. S. Paschen, H. Winkler, T. Nezu, M. Kriegisch, G. Hilscher, J. Custers, and A. Prokofiev, J. Phys: Conf. Ser. **200**, 012156 (2010).

49. T. Takimoto, J. Phys. Soc. Jpn. **80**, 123710 (2011).

50. F. Lu, J. Zhao, H. Weng, Z. Fang, and X. Dai, Phys. Rev. Lett. **110**, 096401 (2013).

51. V. Alexandrov, M. Dzero, and P. Coleman, arXiv: 1303.7224.

52. P. A. Alekseev, V. N. Lazukov, R. Osborn et al., Europhys. Lett. **23**, 347 (1993).

53. P. A. Alekseev, J.-M. Mignot, J. Rossat-Mignot, V. N. Lazukov, and I. P. Sadikov, Physica B **186–188**, 384 (1995).

54. P. Nyhus, S. L. Cooper, Z. Fisk, and J. Sarrao, Phys. Rev. B **55**, 12488 (1997).

55. S. L. Cooper, P. Nyhus, S. Yoon, Z. Fisk, and J. Sarrao, Physica B **244**, 133 (1998).

56. V. N. Antonov, B. Harmon, and A. N. Yaresko, Phys. Rev. B **66**, 165209 (2002).

57. A. Menth, E. Buehler, and T. H. Geballe, Phys. Rev. Lett. **22**, 295 (1969).

58. J. W. Allen, B. Batlogg, and P. Wachter, Phys. Rev. B **20**, (1979).

59. J. C. Cooley, M. C. Aronson, Z. Fisk, and P. C. Canfield, Phys. Rev. Lett. **74**, 1629 (1995).

60. S. Gabani et al., Phys. Rev. B **67**, 172406 (2003).

61. J. C. Cooley, M. C. Aronson, A. Lacerda, Z. Fisk, P. C. Canfield, and R. P. Guerin, Phys. Rev. B **52**, 7322 (1995).

62. A. Yanase and H. Harima, Progr. Theor. Phys. Suppl. **108**, 19 (1992).

63. S. Curnoe and K. A. Kikoin, Phys. Rev. B **61**, 15714 (2000).

64. S. Zhang, Phys. Lett. A **296**, 229 (2002).

65. S. Zhang, Phys. Rev. B **63**, 224402 (2001).

66. T. Caldwell, A. P. Reyes, W. G. Moulton, P. L. Kuhns, J. M. Hoch, P. Schlottmann, and Z. Fisk, Phys. Rev. B **75**, 075106 (2007).

67. S. Wolgast, C. Kurdak, K. Sun, J. W. Allen, D. J. Kim, and Z. Fisk, arXiv:1211.5104.

68. J. Botimer, D. J. Kim, S. Thomas, T. Grant, Z. Fisk, and J. Xin, arXiv:1211.6769.

69. X. Zhang, N. P. Butch, P. Syers, S. Ziemak, R. L. Greene, and J. P. Paglione, arXiv:1211.5532.

70. H. Miyazaki, Tesuya Hajiri, T. Ito, S. Kunii, and S. Kimura, Phys. Rev. B **86**, 075105 (2012).

71. P. Nozières, *Theory of Interacting Fermi Systems*, Benjamin, New York (1964).

72. M. Neupane et al., arXiv:1306.4634.

73. J. Jiang et al., arXiv:1306.5664.

74. G. Li et al., arXiv:1306.5221.

75. D. J. Kim, J. Xia, and Z. Fisk, arXiv:1307.0448.

76. S. Thomas, D. J. Kim, S. B. Chung et al., arXiv:1307.4133.